

CMB ANOMALIES FROM IMPERFECT DARK ENERGY: CONFRONTATION WITH THE DATA

MAGNUS AXELSSON¹, FRODE HANSEN¹, TOMI KOIVISTO^{1,2}, DAVID F. MOTA¹

¹ Institute of Theoretical Astrophysics, University of Oslo, P.O. Box 1029 Blindern, N-0315 Oslo, Norway

² Institute for Theoretical Physics and the Spinoza Institute, Utrecht University, Leuvenlaan 4, Postbus 80.195, 3508 TD Utrecht, The Netherlands

(Dated: February 25, 2024)
 Draft version February 25, 2024

ABSTRACT

We test anisotropic dark energy models with the 7-year WMAP temperature observations data. In the presence of imperfect sources, due to large-scale gradients or anisotropies in the dark energy field, the CMB sky will be distorted anisotropically on its way to us by the ISW effect. The signal covariance matrix then becomes nondiagonal for small multipoles, but at $\ell \gtrsim 20$ the anisotropy is negligible. We parametrize possible violations of rotational invariance in the late universe by the magnitude of a post-Friedmannian deviation from isotropy and its scale dependence. This allows to obtain hints on possible imperfect nature of dark energy and the large-angle anomalous features in the CMB. A robust statistical analysis, subjected to various tests and consistency checks, is performed to compare the predicted correlations with those obtained from the satellite-measured CMB full sky maps. The preferred axis point towards $(l, b) = (168^\circ, -31^\circ)$ and the amplitude of the anisotropy is $\varpi_0 = (0.51 \pm 0.94)$ (1σ deviation quoted). The best-fit model has a steep blue anisotropic spectrum ($n_{\text{de}} = 3.1 \pm 1.5$).

Subject headings: cosmic microwave background — cosmology: observations — methods: numerical

1. INTRODUCTION

In the past two decades great advances have been made in observational cosmology. The most striking single discovery is the present acceleration of the universe expansion, now confirmed by many independent experiments. The most powerful probe of precision cosmology is the observations of the cosmic microwave background (Bennett et al. (2003); Hinshaw et al. (2007)), which seem to support the model of universe which at large scales is flat, isotropic and homogeneous, as firmly predicted by inflation. However, at more subtle level there seems to be also hints of substantial anisotropy. Such would imply violation of the cosmological principle, perhaps as striking change of paradigm as the introduction of dark energy. Presently the evidence for anisotropy is debatable, but the bounds can definitely be expected to improve with the Planck experiment. Therefore it is extremely interesting to study theoretical links between the acceleration and anisotropies, in particular, the possibility to constrain them observationally Copi et al. (2010).

Several distinct statically anisotropic features have been reported in the data analysis of the CMB sky. Among the most curious is the presence of hemispherical asymmetry (Eriksen et al. (2004)). Recent investigations exploiting the five-year WMAP data have found that the evidence for this asymmetry is increasing and extends to much smaller angular scales than previously believed to (Hansen et al. (2008); Hoftuft et al. (2009)). Alignment of the quadrupole and octupole, the so called Axis of Evil (Land & Magueijo (2005)) could also seem an unlikely result of statistically isotropic perturbations, even without taking into account that these multipoles happen also to be aligned to some extent with the dipole and with the equinox. In the CMB spectrum, the angular correlation spectrum seems to be lacking power at the largest scales. The alignments seem to be statistically indepen-

dent of the the lack of angular power (Rakic & Schwarz (2007)). For other studies, see (Prunet et al. (2005); Gordon et al. (2005)).

It is natural to associate the apparent statistical anisotropy with dark energy, since the anomalies occur at the largest scales, and these enter inside the horizon at the same epoch that the dark energy dominance begins. The paramount characteristic of dark energy is its negative pressure. One may then contemplate whether this pressure might vary with the direction. Then also the universal acceleration becomes anisotropic, and one would indeed see otherwise unexpected effects. These would presumably be strongest at the smallest multipoles of the CMB since they describe the large angular scales which are most directly affected during the late epochs of the universe. Specifically, as the photons travel from the last scattering surface towards us, the their temperature gets blue- and redshifted as they fall in and climb out of the gravitational wells, respectively. When the potentials evolve, there is a net effect in the temperature of the photons: this is the integrated Sachs-Wolfe effect (ISW). Furthermore, if the average evolution of the potentials was not the same in different directions of the sky, the effect would be anisotropic. However, to explain the lack of large-angle correlations, there should occur a cancellation with the Sachs-Wolfe effect from the potentials last scattering surface that typically contribute to the large angles with similar order of magnitude as the ISW Afshordi et al. (2009).

The potentials parameterising the perturbations of the metric, can be written in the longitudinal gauge as

$$ds^2 = a^2(\eta) [-(1 + 2\psi)d\eta^2 + (1 - 2\phi)dx^i dx_i]. \quad (1)$$

The Poisson equation relates the spacetime curvature ϕ to the matter sources. As is well known, in the absence of anisotropic stress the potentials ϕ and ψ are

equal. Thus, detection of inequality of these potentials in the present universe would indicate the presence of imperfect energy source, either in form of dark energy fluid or modification of gravity (Koivisto & Mota (2006); Daniel et al. (2008); Manera & Mota (2006); Dvali et al. (2000)). Clearly, the difference of the potentials can be constrained much tighter at Solar system than at cosmological scales (Mota et al. (2007); Daniel et al. (2009); Ferreira & Skordis (2010); Skordis (2009); Hu & Sawicki (2007)). In the present study, we consider the possibility that the relation of the anisotropy described by the difference of the potentials does not cancel out on the average, i.e. that the anisotropy is statistical.

This amounts to promoting each Fourier mode of the potentials to depend not only on the length but also on the direction of the wavevector. This is a generic prediction for perturbations in a non-FRW universe and also for non-scalar field models, in particular vector fields Armendariz-Picon (2004); Koivisto & Mota (2008a); Zuntz et al. (2010); Li et al. (2008). It has been considered if the cosmological fine-tunings could be more naturally alleviated with a dynamical dark energy component when this is modelled with a more general field than a scalar. Vector fields dynamics could accelerate the universe today (Kiselev (2004); Jimenez & Maroto (2008)) having phantom evolution without UV pathology (Rubakov (2006); Libanov et al. (2007)) possibly connecting the acceleration with the electromagnetic scale (Jimenez & Maroto (2009a,b); Jimenez et al. (2009)).

There has also been interest on anisotropies in inflation (Gumrukcuoglu et al. (2006); Ackerman et al. (2007); Boehmer & Mota (2008)), and their comparison with the data (Groeneboom & Eriksen (2008); Groeneboom et al. (2010); Armendariz-Picon & Pekowsky (2008)). The anisotropy in the primordial spectrum could be generated by vector fields (Golovnev et al. (2008); Koivisto & Mota (2008b)) or more general n-forms (Germani & Kehagias (2009); Koivisto et al. (2009); Koivisto & Nunes (2009)). In particular this can be robustly realized by the vector curvaton paradigm (Dimopoulos et al. (2010)) which Dimopoulos et al. (2011) recently implemented within D-brane inflation in type II string theory by taking into account the $U(1)$ gauge field that lives on the brane. Perturbations have been also studied in anisotropically inflating backgrounds (Pereira et al. (2007); Gumrukcuoglu et al. (2007)) and in the shear-free cosmologies considered in Koivisto et al. (2011); Zlosnik (2011), where the expansion is isotropic but the spatial curvature depends on the direction. These homogeneous but anisotropic universes could emerge by tunneling from a lower-dimensional vacuum Adamek et al. (2010); Graham et al. (2010).

In the presence of such variety of possibilities, we choose to rather employ a general parametrisation than study a particular model. To that purpose, we parameterize directly the angular variation of the gravitational potentials. This can be seen as a step towards a more complete anisotropic post-Friedmannian parametrisation of the deviations from standard GR Λ CDM cosmology, inspired by the recent development of a fully consistent parametrisation encompassing statistically isotropic models (Ferreira & Skordis (2010); Baker et al. (2011)). In Section 2 we derive the signal covariance matrix in the presence of generalised perturbation sources. In Sec-

tion 3 we describe our parametrisation of such sources and their interpretation as anisotropies of the dark energy field or as some spontaneous anisotropisation of the CMB radiation. In Section 4 we discuss the analysis, and the method we use is described in detail in Section 4, and finally, the results are presented in Section 5.

2. CMB FROM ANISOTROPIC SCALAR SOURCES

The temperature anisotropy field is conventionally expanded in terms of the spherical harmonics and on the other hand considered in the Fourier space

$$\Theta(\mathbf{x}, \hat{e}, \eta) = \sum_{\ell=0}^{\infty} \sum_{m=-\ell}^{\ell} a_{\ell m} Y_{\ell m} = \int \frac{d^3 k}{(2\pi)^3} e^{i\mathbf{k} \cdot \mathbf{x}} \delta(\mathbf{k}) \Theta(\mathbf{k}, \hat{e}, \eta), \quad (2)$$

where we have normalized the transfer function $\Theta(\mathbf{k}, \mathbf{e}, \eta)$ with respect to the initial amplitude $\delta(\mathbf{k})$. One makes contact between the two expansions by using the Rayleigh formula

$$e^{i\mathbf{x} \cdot \mathbf{k}} = \sum_{\ell=0}^{\infty} i^{\ell} (2\ell + 1) j_{\ell}(kx) Y_{\ell m}^*(\hat{k}) Y_{\ell m}(\hat{x}), \quad (3)$$

together with the addition theorem for the spherical harmonics

$$P_{\ell}(\hat{k} \cdot \hat{p}) = \frac{4\pi}{2\ell + 1} \sum_{m=-\ell}^{\ell} Y_{\ell m}^*(\hat{k}) Y_{\ell m}(\hat{p}) \quad (4)$$

for the second equality in Eq.(2) and then, by exploiting the orthonormality of the spherical harmonics, picks up the coefficients in the first equality in Eq.(2). These are

$$a_{\ell m} = i^{\ell} \int \frac{d^3 k}{2\pi^2} \delta(\mathbf{k}) Y_{\ell m}^*(\hat{k}) \Theta_{\ell}(\mathbf{k}). \quad (5)$$

where we have defined

$$\Theta_{\ell}(\mathbf{k}) = \int j_{\ell}(kr(\eta)) \Theta(\mathbf{k}, \eta) d\eta. \quad (6)$$

We assume, as usual, that the primordial spectrum of perturbations is statistically isotropic,

$$\langle \delta(\mathbf{k}) \delta^*(\mathbf{k}') \rangle = P(k) (2\pi)^3 \delta^3(\mathbf{k} - \mathbf{k}'). \quad (7)$$

However, we allow the transfer function an anisotropic part,

$$\Theta_{\ell}(\mathbf{k}) = \Theta_{\ell}^0(k) + \omega(\hat{k} \cdot \hat{n}) \Theta_{\ell}^A(k). \quad (8)$$

The second term can then incorporate the anisotropic ISW contribution from dark energy. We are then interested in the correlators

$$\langle a_{\ell m} a_{\ell' m'}^* \rangle = \frac{2i^{\ell-\ell'}}{\pi} \int d^3 k P(k) Y_{\ell m}^*(\hat{k}) Y_{\ell' m'}(\hat{k}) \Theta_{\ell}(\mathbf{k}) \Theta_{\ell'}^*(\mathbf{k}). \quad (9)$$

The expression follows directly from Eq.(5). One may arrive at the same result by inverting Eq.(2) to obtain the $a_{\ell m}$, expanding $\Theta(\mathbf{k}, \hat{e}, \eta)$ as a Legendre series and using the addition theorem (4) to eliminate the Legendre polynomials P_{ℓ} when integrating over the direction in the sky.

It is useful to introduce the spherical components as in Ackerman et al. (2007) of the direction vector

$$n_{\pm} = \mp \left(\frac{\hat{n}_x \mp i\hat{n}_y}{\sqrt{2}} \right), \quad n_0 = \hat{n}_z, \quad (10)$$

since then one may write

$$\hat{k} \cdot \hat{n} = 2\sqrt{\frac{\pi}{3}} \left[n_+ Y_1^{+1}(\hat{k}) + n_- Y_1^{-1}(\hat{k}) + n_0 Y_1^0(\hat{k}) \right]. \quad (11)$$

We arrive at

$$\langle a_{\ell m} a_{\ell' m'}^* \rangle = \frac{2i^{\ell-\ell'}}{\pi} \left[\delta_{m',m} \delta_{\ell',\ell} I_{\ell} + \zeta_{\ell m; \ell' m'} I_{\ell \ell'}^A + \xi_{\ell m; \ell' m'} I_{\ell \ell'}^{AA} \right]. \quad (12)$$

Here the source integrals are

$$I_{\ell} = \int_0^{\infty} dk k^2 P(k) [\Theta_{\ell}^0(k)]^2, \quad (13)$$

$$I_{\ell \ell'}^A = \int_0^{\infty} dk k^2 P(k) [\omega \Theta_{\ell'}^0(k) \Theta_{\ell}^A(k) + \omega^* \Theta_{\ell}^0(k) \Theta_{\ell'}^A(k)], \quad (14)$$

and

$$I_{\ell \ell'}^{AA} = \int_0^{\infty} dk k^2 P(k) |\omega|^2 \Theta_{\ell}^A(k) \Theta_{\ell'}^A(k). \quad (15)$$

The first term in Eq.(12) is the isotropic contribution. The second is the cross term, for which the geometric coefficients are given by

$$\zeta_{\ell m; \ell' m'} = n_+ \zeta_{\ell m; \ell' m'}^+ + n_- \zeta_{\ell m; \ell' m'}^- + n_0 \zeta_{\ell m; \ell' m'}^0, \quad (16)$$

where

$$\zeta_{\ell m; \ell' m'}^+ = \delta_{m', m-1} \left[\delta_{\ell', \ell-1} \sqrt{\frac{(\ell+m-1)(\ell+m)}{2(2\ell-1)(2\ell+1)}} - \delta_{\ell', \ell+1} \sqrt{\frac{(\ell-m+1)(\ell-m+2)}{2(2\ell+1)(2\ell+3)}} \right], \quad (17)$$

$$\zeta_{\ell m; \ell' m'}^- = \delta_{m', m+1} \left[\delta_{\ell', \ell-1} \sqrt{\frac{(\ell-m-1)(\ell-m)}{2(2\ell-1)(2\ell+1)}} - \delta_{\ell', \ell+1} \sqrt{\frac{(\ell+m+1)(\ell+m+2)}{2(2\ell+1)(2\ell+3)}} \right], \quad (18)$$

$$\zeta_{\ell m; \ell' m'}^0 = \delta_{m', m} \left[\delta_{\ell', \ell-1} \sqrt{\frac{(\ell-m)(\ell+m)}{(2\ell-1)(2\ell+1)}} + \delta_{\ell', \ell+1} \sqrt{\frac{(\ell-m+1)(\ell+m+1)}{(2\ell+1)(2\ell+3)}} \right]. \quad (19)$$

One can check that $\zeta_{\ell m; \ell' m'}^* = \zeta_{\ell' m'; \ell m}$. The last term in Eq.(12) is the autocorrelation of the anisotropic piece. The geometric coefficients $\xi_{\ell m; \ell' m'}$ have been previously presented in Ackerman et al. (2007). We have them with an extra minus sign for the off-diagonal components¹. The factor $i^{\ell-\ell'}$ also results in odd-parity correlations being imaginary.

Although our cosmology features anisotropies, we assume that the underlying model is Gaussian. For a pedagogic discussion of these statistical properties and their tests, see Abramo & Pereira (2010).

3. ANISOTROPICALLY STRESSED DARK ENERGY

The main reason for disregarding the anisotropic stress in the dark energy fluid might be that a minimally coupled scalar field, conventional parametrisation of the inflationary energy source, cannot generate anisotropic stresses. However, since there is no fundamental theoretical model to describe dark energy, one might miss the behind physics of acceleration by sticking to the assumption of zero anisotropic stress. Such stresses are quite by viscous fluids, any higher spin fields and non-minimally coupled scalar fields too Appleby et al. (2010); Battye & Moss (2009); Rodrigues (2008); Campanelli (2009); Dimastrogiovanni et al. (2008); Cooray et al. (2008); Akarsu & Kilinc (2010); Cooke & Lynden-Bell

(2009). To study such a generic property with a many possible theoretical realizations, it is useful to employ a parametrisation of its physical consequences.

An efficient way to describe possible deviations from perfect-fluid cosmology is to introduce the post-general relativity cosmological parameter ϖ along the lines of Caldwell et al. (2007), which is defined as the difference of gravitational potentials in the Newtonian gauge,

$$\psi = (1 + \varpi)\phi, \quad (20)$$

where the line element reads

$$ds^2 = a^2(\eta) [-(1 + 2\psi)d\eta^2 + (1 - 2\phi)dx^i dx_i], \quad (21)$$

This parameter then appears as a cosmological generalization of the post-Newtonian γ , for which one has tight constraints from the Solar system scales Will (2001). An economic assumption is then that such a generalized parameter depends, at all relevant scales, on the ratio of matter and dark energy densities,

$$\varpi = \varpi_0 \frac{\rho_{DE}}{\rho_M}. \quad (22)$$

Then one has reasonable constraints on the ϖ_0 from various scales, and ϖ_0 of order one would imply a variety of phenomenology at different scales, ranging from Solar system physics to cosmology, just at the verge of detection. Here we study on cosmological effects of dark energy and adopt the recipe 3 of Caldwell et al. (2007) as the basis to parametrize the shear stress of dark energy.

In particular, we will explore the case that the anisotropic stress has a preferred direction as in

¹ The reason for this discrepancy was a forgotten $i^{\ell-\ell'}$ factor in the Ackerman paper.

Koivisto & Mota (2008a). For each Fourier mode of cosmological perturbations, we write

$$\varpi = i(\hat{k} \cdot \hat{n})\varpi_0 \frac{\rho_{DE}}{\rho_M}, \quad (23)$$

where \hat{n} is the direction of the anisotropy and ϖ_0 is real. Consider then the transfer function Eq.(8). The $\Theta_\ell^0(k)$ would now be as usual. Thus it includes contributions from both early and late universe. At the largest scales the Sachs-Wolfe effects are known to dominate the anisotropy sources. The second part would be given by the rotationally non-invariant part of the ISW contribution, which in our present prescription is the following:

$$\Theta_\ell^A(k) = -i\varpi_0 \int e^{-\kappa(\eta)} \frac{d}{d\eta} \left(\frac{\rho_{DE}}{\rho_M} \phi_k(\eta) \right) j_\ell[kr(\eta)] d\eta, \quad (24)$$

where $\phi_k(\eta)$ is given by the standard computation. We just add the extra contributions due to Eq.(24) to the sources from which to compute the correlators as described in the previous section. Therefore it becomes straightforward to determine the features in the CMB sky in this prescription.

This parametrization describes a gradient-type modification of the effective CMB sources. We note that Tangen (2009) has determined the implications of a super-horizon perturbation, and Erickcek et al. (2008) considered such a spatial variation of the curvature field at inflation. In our model, the anisotropy is formed dynamically and becomes important with the dominance of dark energy. Explicitly, we have a spontaneous modification of the effective CMB sources through the gradient operator as follows:

$$\psi(\mathbf{x}) = [1 + (\mathbf{n} \cdot \nabla)] \phi(\mathbf{x}) \quad (25)$$

when $|n| = \varpi_0(\rho_{DE}/\rho_M)$. This amounts to shifting the Fourier modes of the perturbations exactly as prescribed in (20) and (23),

$$\psi_{\mathbf{k}} = \left[1 + i(\hat{k} \cdot \hat{n})\varpi_0 \frac{\rho_{DE}}{\rho_D} \right] \phi_{\mathbf{k}}. \quad (26)$$

Since the anisotropic part develops as a result of the evolution of the universe, it is a property of the transfer functions and not of the primordial spectrum of perturbations. One does not expect odd $\Delta\ell$ couplings from primordial origin, since they violate parity. The presence of the imaginary unit is necessary for reality of the perturbations, which can be checked as follows. Since the physical perturbation is a convolution of the primordial physical perturbation and the Fourier transformation of the transfer function, one notes that the latter should also be real. We get that

$$\frac{\psi(\mathbf{x})}{\psi_{\text{Primordial}}(\mathbf{x})} = \frac{1}{2\pi^3} \int_0^\infty dk \frac{k}{x} \sin(kx) \left[1 + (\hat{x} \cdot \hat{n}) \left(\frac{1}{kx} - \cot(kx) \right) \right] \phi(k), \quad (27)$$

where $\phi(k)$ is the (real, isotropic) transfer function which depends only on the magnitude of the wavevector, and the right hand side is the anisotropic transfer function in the configuration space that retains its reality.

To recap our approach, we introduced a mismatch of the two gravitational potentials in the Newtonian gauge. This mismatch, quantified by ϖ , is given by a gradient along a preferred axis \hat{n} . In the following, we will also allow scale dependence of this effect by introducing the spectral index n_{de} . This parametrisation can then be used to constrain the presence of the such gradients in the late universe, since they would be seen in the CMB (practically only) through their impact on the time-evolution of the gravitational potentials because of the ISW effect. Physically, these gradients could be caused by a large-scale inhomogeneity entering our horizon, spontaneous formation due to e.g. coherent magnetic fields or simply the possible imperfect nature of the dark energy field.

To clarify the difference of our approach to all previous literature, let us mention that odd modulations may be considered to occur at three distinct levels. The temperature field itself can be modulated, for a recent example see Aluri & Jain (2011). This would effectively describe some systematics in the data. Strangely enough, the primordial spectrum itself could contain parity violating contribution Koivisto & Mota (2011). That is consistent only in the context of noncommutative quantum field theory, and thus provides a unique signal for such high energy modifications of the standard model Groeneboom et al. (2010). Finally, the cosmological structures may evolve statistically oddly, which is the case we focus upon here.

4. MODEL FITTING

In this section we describe in detail the confrontation of the model with the WMAP data. We will now discuss the method used to obtain the set of parameters which gives the best fit between our model and the observations. Our basis is the evaluation of the Likelihood function in a 4-dimensional parameter space. After explaining the general likelihood procedure, we explain in more detail the different steps taken to calculate and maximize the likelihood.

4.1. Data model and notation

Given a set of data $\{d_i\}$ our goal is to find the set of parameters which maximizes the posterior. For ease of notation let $\alpha = (\theta, \phi, \varpi_0, n_{de}) = (\hat{\mathbf{n}}, \varpi_0, n_{de})$ denote the set of parameters to be determined. By Bayes' theorem we know that the posterior distribution $P(\alpha|\mathbf{d}) \propto \mathbf{P}(\mathbf{d}|\alpha)\mathbf{P}(\alpha) = \mathcal{L}(\alpha)\mathbf{P}(\alpha)$ where $\mathcal{L}(\alpha)$ is the likelihood and $P(\alpha)$ is a prior. We take a conservative approach and assume that we know nothing prior about the anisotropic parameters, and thus $P(\alpha|\mathbf{d}) = \mathcal{L}(\alpha)$ up to a normalization constant. If we manage to compute the likelihood function in all of the parameter space then we automatically have the posterior distribution and our job is essentially done.

Although our model is anisotropic we still assume that the underlying distribution is Gaussian, and thus the likelihood is

$$\mathcal{L}(\alpha) \propto \frac{e^{-\frac{1}{2}\mathbf{d}^\dagger \mathbf{C}^{-1}(\alpha)\mathbf{d}}}{\sqrt{\det \mathbf{C}(\alpha)}} \quad (28)$$

where the data vector \mathbf{d} consists of the $a_{\ell m}$ of the observed masked map. The correlation matrix $\mathbf{C} = \mathbf{S} + \mathbf{N}$ is the sum of the CMB signal covariance matrix \mathbf{S} and the

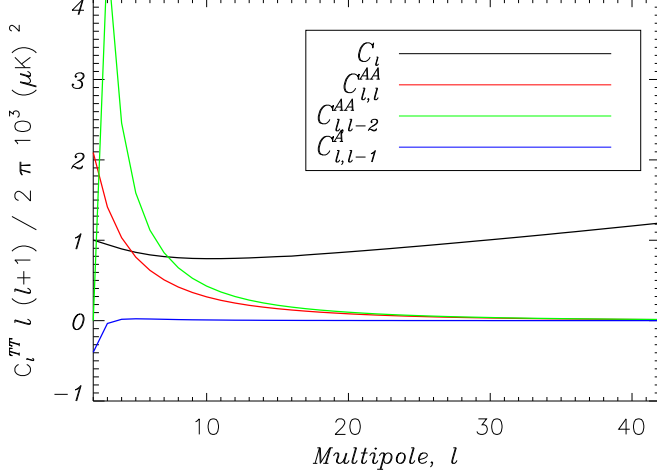


FIG. 1.— (Unnormalized) Integrals (eq. 31 - 33) computed from a modified version of CAMB Lewis et al. (2000). Notice how the anisotropic integrals decay towards zero after only a few multipoles. These integrals are all used in the construction of the signal covariance matrix. An anisotropic scalar spectral index of $n_{de} = 1.0$ is used in this plot, and we have not normalized them. (Color version of this figure is available online)

noise covariance matrix \mathbf{N} . Our analysis is performed in harmonic space where the signal covariance $S_{\ell m; \ell' m'} = \langle a_{\ell m} a_{\ell' m'}^* \rangle$ is computed from Eq. (12) and thus contains non-diagonal anisotropic contributions from dark energy. This matrix gives the dependence on the cosmological parameters.

Finally the observed data vector \mathbf{d} may be written in harmonics space as

$$\mathbf{d}_{\ell m} = b_{\ell} w_{\ell} s_{\ell m} + n_{\ell m} \quad (29)$$

where b_{ℓ} is the instrumental beam, w_{ℓ} is the pixel window function and $n_{\ell m}$ is the (Gaussian) noise term. Since there is no correlation between the signal and the noise we have

$$\langle d_{\ell m} d_{\ell' m'}^* \rangle = \langle \tilde{s}_{\ell m} \tilde{s}_{\ell' m'}^* \rangle + \langle n_{\ell m} n_{\ell' m'}^* \rangle \quad (30)$$

where $\tilde{s}_{\ell m} = b_{\ell} w_{\ell} s_{\ell m}$ is the observed signal. The goal is now to maximize this likelihood with respect to the model parameters, but we will first explain in some detail how we calculate the covariance matrices involved in the likelihood calculation.

4.2. Signal covariance

From equations (12-19) we see that the covariance matrix, in addition to the diagonal isotropic contribution I_{ℓ} contains the cross term coefficients $\xi_{\ell m; \ell' m'}$ which couple ℓ to $\ell' = [\ell \pm 1]$ and m to $m' = [m, m \pm 1]$. The last term $\xi_{\ell m; \ell' m'}$ is the Ackerman (Ackerman et al. 2007) term for which we have couplings when $\ell' = [\ell, \ell \pm 2]$ with $m' = [m, m \pm 1, m \pm 2]$. All other terms are zero.

We will now express the integrals in equations (17-19) in terms of power spectra C_{ℓ} , $C_{\ell\ell'}^A$, $C_{\ell\ell'}^{AA}$ as

$$C_{\ell} = \frac{2}{\pi} I_{\ell\ell} \quad (31)$$

$$C_{\ell\ell'}^A = \frac{2}{\pi} I_{\ell\ell'}^A \quad (32)$$

$$C_{\ell\ell'}^{AA} = \frac{2}{\pi} I_{\ell\ell'}^{AA} \quad (33)$$

From equations (17-19) we see that $C_{\ell\ell'}^A$ and $C_{\ell\ell'}^{AA}$ only give contributions for $\ell' = \ell \pm 1$ and $\ell' = \ell \pm 2$. In figure 1 we have calculated (using a modified version of CAMB) and plotted these integrals (because of symmetry the $\ell' = \ell + 1$ and $\ell' = \ell + 2$ terms are equal to the $\ell' = \ell - 1$ and $\ell' = \ell - 2$ terms plotted) and compared to the isotropic power spectrum. From this figure we clearly see that the anisotropic contribution from the dark energy component becomes negligible except at the largest scales where the anisotropic contribution even exceeds the isotropic. The most prominent alteration comes from the anisotropic integral $C_{\ell, \ell-2}^{AA}$ contributing to the off-diagonal elements of the signal covariance matrix. Due to the short range of the anisotropic integrals we have altered the pivot scale in CAMB from $k_0 = 0.05 \text{ Mpc}^{-1}$ to $k_0 = 2 \times 10^{-3} \text{ Mpc}^{-1}$. In this way, we ensure that the spectral index enters correctly to tilt these integrals.

4.3. Transformation of variables

We have noticed from simulations that there was a significant degeneration between the anisotropic spectral index n_{de} and the amplitude ϖ_0 due to the fact that they both regulate the magnitude of the non-diagonal signal matrix elements. In order to ease the estimation procedure, we choose to estimate for a new variable ϖ_0^a instead of ϖ_0 defined by $\varpi_0^a = \varpi_0 / \sqrt{a}$ where we define a as $a = A(I_{\ell\ell-2}^{AA}(1.0)) / A(I_{\ell\ell-2}^{AA}(n_{de}))$ where $A(I_{\ell\ell'}^X(n_{de}))$ is the area under the anisotropic integral $I_{\ell\ell'}^X(n_{de})$ where $X = \{A, AA\}$ and n_{de} is the dark energy spectral index. The parameters n_{de} and ϖ_0^a are not degenerate and can thus more easily be estimated for. In the end, we convert to the physical parameter ϖ_0 and all results are quoted in terms of this parameter.

4.4. Modification of spectrum

The angular power spectrum C_{ℓ} will receive a contribution from the anisotropy which could have an observable impact on the largest scales of the universe. This can be seen from equations (17-19) and the form of the $\xi_{\ell m; \ell' m'}$ elements (see Ackerman et al. (2007) for details). One must therefore be careful when performing the full analysis, making sure that any choice for ϖ_0 does not significantly affect the power spectrum away from the WMAP best fit spectrum, but only the anisotropic contribution to the correlations between $a_{\ell m}$ s.

To quantize these statements we calculate the net extra power from the anisotropic contribution. It is given by the diagonal part of the anisotropy which can be written

$$\Delta C_{\ell} = \frac{2 I_{\ell\ell}^{AA}}{\pi} \frac{\varpi_0^2}{2\ell + 1} \sum_{m=-\ell}^{\ell} \xi_{\ell m; \ell m} \quad (34)$$

Using the explicit form of $\xi_{\ell m; \ell m}$ to perform the summation we find the modified power spectrum (see the Appendix for details):

$$C_{\ell}^{\text{mod}} = C_{\ell} + \frac{2}{3\pi} \varpi_0^2 I_{\ell\ell}^{AA}(n_{de}) \equiv C_{\ell} + \frac{\varpi_0^2}{3} C_{\ell}^{AA} \quad (35)$$

The extra contribution to the power-spectrum from the anisotropic sources depends on the amplitude parameter ϖ_0 (degree of isotropy breaking) and the dark energy

spectral index (parameterisation of the fluid scale-dependence) which we have included explicitly as an argument in $I_{\ell\ell}^{\text{AA}}$.

We see from equation 35 that there is a limit to what values the amplitude ϖ_0 may take in order to obtain a power spectrum which is consistent with the WMAP7 best fit. This is however only true when we assume the other cosmological parameters to have the WMAP best fit values. Clearly the new parameters which we have introduced allows for the other parameters to vary and one should re-estimate the other cosmological parameters together with ϖ_0 and n_{de} . In order to test the anisotropic model without running a full cosmological parameter estimation one may renormalize the covariance matrix for a given set of parameters (ϖ_0, n_{de}) in such a way that the power spectrum is kept constant at the best fit WMAP model. In this case the signal covariance becomes

$$S_{\ell m; \ell' m'}^{\text{Norm}} = \left(\frac{S_{\ell m; \ell' m'}}{\sqrt{S_{\ell m; \ell m} S_{\ell' m'; \ell' m'}}} \right) C_{\ell} \quad (36)$$

$$N_{\ell_1 m_1; \ell_2 m_2} = (-1)^{m_1} \sqrt{\frac{(2\ell_1 + 1)(2\ell_2 + 1)}{4\pi}} \sum_{\ell_3=0}^{2\ell_{\text{max}}} a_{\ell_3 m_3} \sqrt{2\ell_3 + 1} \begin{pmatrix} \ell_3 & \ell_1 & \ell_2 \\ 0 & 0 & 0 \end{pmatrix} \begin{pmatrix} \ell_3 & \ell_1 & \ell_2 \\ m_3 & -m_1 & m_2 \end{pmatrix} \delta(m_3 - m_1 + m_2) \quad (37)$$

where the Dirac delta-function arises due to the requirement $m_1 - m_2 - m_3 = 0$ for the Wigner $3j$ symbols. It is also required that the triangle condition $|\ell_1 - \ell_2| \leq \ell_3 \leq \ell_1 + \ell_2$ is fulfilled. Notice also that due to this relation the sum over ℓ_3 goes up to $2\ell_{\text{max}}$.

The $a_{\ell_3 m_3}$ coefficients originate from a spherical transform of the variance of the noise map, σ_i^2 . Eq. (37) is then implemented into our code. It needs only be computed once for each run of the code and is added to the signal covariance matrix in the step before the skycut is applied.

4.6. Correlations introduced by the mask

If we let $C_{\ell m; \ell' m'}$ denote the covariance matrix without mask, and $\tilde{C}_{\ell m; \ell' m'}$ denote the corresponding matrix including correlations from the sky cut, then the relation between them in harmonic space is found to be

$$\tilde{C}_{\ell m; \ell' m'} = \sum_{LM} \sum_{L'M'} W_{\ell m; LM} C_{LM; L'M'} W_{\ell' m'; L'M'}^* \quad (38)$$

which can be written compactly in matrix form as $\tilde{\mathbf{C}} = \mathbf{WCW}^\dagger$. The operation in Eq. (38) can be shown to be additive so the covariance matrix is the sum of the signal plus noise correlation matrices. The multipole range here is $L, L' \in [2, \ell_{\text{max}}]$, and the sums over M, M' here run over positive values. The hermitean coupling matrix $W_{\ell m; \ell' m'}$ defined by

$$W_{\ell m; \ell' m'} = \int d\Omega M(\Omega) Y_{\ell m}^*(\Omega) Y_{\ell' m'}(\Omega) \quad (39)$$

is a function of the pixel space mask $M(\Omega)$ (where $\Omega = (\theta, \phi)$ is the angular position on the sky) and so depends on the resolution N_{side} . It quantifies the new couplings between modes that arise due to the fact that we are now not analyzing a full sky.

where $S_{\ell m; \ell m} = C_{\ell} + \xi_{\ell m; \ell m} \varpi_0^2 C_{\ell}^{\text{AA}}$. With this normalization, the diagonal part of our signal covariance matrix will match the WMAP power spectrum regardless of amplitude and spectral index for the dark energy, while the off-diagonal components describe relative anisotropy.

4.5. Noise covariance

The noise in pixel space is assumed to be uncorrelated between pixels, *i.e.* $\mathbf{N}_{ij} = \langle n_i n_j \rangle = \sigma_i^2 \delta_{ij}$ where i and j are pixel indices, and σ_i is the noise root-mean-square deviation. The noise covariance matrix in pixel space is therefore diagonal. When going to spherical harmonic space, the harmonic coefficients of the noise are correlated and $N_{\ell m; \ell' m'} = \langle n_{\ell m} n_{\ell' m'}^* \rangle$ is therefore a dense matrix.

Expanding the noise harmonic coefficients in terms of pixel space quantities we eventually find that the expression for the noise matrix in harmonic space becomes

Starting with the WMAP KQ85 mask at $N_{\text{side}} = 512$ we degrade our mask so that the operation of applying the mask in pixel space can be traced exactly by applying the kernel matrix \mathbf{W} in harmonic space. This is done by first smoothing with a Gaussian beam of $\text{fwhm} = 744$ arcmin, and then setting $M(p) = 0$ (where p is a HEALPix pixel index) where $M(p) < 0.80$. We then band-limit the mask so that it contains multipoles in the desired range (Armendariz-Picon & Pekowsky 2008). These operations ensure that our mask does not contain small-scale structures. In the process the mask is expanded so that it now covers about 25% of the sky.

It now remains to give an expression for the coupling kernel. Eq. (39) can be transformed by decomposing the mask into spherical harmonics and then performing the resulting integral over all angles to obtain again Wigner $3j$ symbols. This is exactly the same analytical procedure which led to Eq. (37) with some minor modifications. The result in this case becomes

$$W_{\ell_1 m_1; \ell_2 m_2} = (-1)^{m_2} \sqrt{\frac{(2\ell_1 + 1)(2\ell_2 + 1)}{4\pi}} \sum_{\ell_3=0}^{2\ell_{\text{max}}} a_{\ell_3 m_3} \sqrt{2\ell_3 + 1} \begin{pmatrix} \ell_3 & \ell_1 & \ell_2 \\ 0 & 0 & 0 \end{pmatrix} \begin{pmatrix} \ell_3 & \ell_1 & \ell_2 \\ m_3 & m_1 & -m_2 \end{pmatrix} \delta(m_3 + m_1 - m_2) \quad (40)$$

almost identical with Eq. (37). As in the previous case the internal sum covers multipoles up to $2\ell_{\text{max}}$, and the main difference is a change in sign of m_1, m_2 . We find that the mask coupling matrix is relatively well conditioned and further manipulations are not necessary. This has been tested by simply inverting the kernel matrix \mathbf{W} constructed from the resulting mask which is used in the analysis of the WMAP data.

4.7. Likelihood maximization scheme

In order to maximize the likelihood we use a non-linear Newton-Rapson search algorithm² for the direction and amplitude. Finding the maximum of the likelihood is equivalent to finding the minimum of the quantity

$$-2 \log \mathcal{L} = \mathbf{d}^\dagger \mathbf{C}^{-1} \mathbf{d} + \text{Tr} \log \mathbf{C}. \quad (41)$$

which has a global minimum when the likelihood function has a global maximum. The algorithm minimizes a general unconstrained function by evaluating the first

$$\frac{\partial(-2 \log \mathcal{L})}{\partial \alpha} = \mathbf{d}^\dagger \frac{\partial \mathbf{C}^{-1}}{\partial \alpha} \mathbf{d} + \text{Tr} \left(\frac{\partial \log \mathbf{C}}{\partial \alpha} \right) = -\mathbf{d}^\dagger \mathbf{C}^{-1} \frac{\partial \mathbf{C}}{\partial \alpha} \mathbf{C}^{-1} \mathbf{d} + \text{Tr} \left(\mathbf{C}^{-1} \frac{\partial \mathbf{C}}{\partial \alpha} \right) \quad (42)$$

To find the derivative of \mathbf{C}^{-1} we have differentiated the identity matrix $\mathbf{I} = \mathbf{C}\mathbf{C}^{-1}$ and solved for the derivative of the inverse covariance matrix in terms of the derivative of the matrix itself. The analytic derivative of \mathbf{C} is computed from Eq. 12. The second derivatives are estimated from the gradient using a secant method. Depending on our initial guess for the parameters and our convergence criteria the minimizer in general may or may not converge to a global minimum. In our case false convergence is rarely a problem since the likelihood surface is well behaved and the local minimum has a small amplitude compared to the global.

For the spectral index n_{de} we run a grid calculation. In each grid point, we apply the above maximization procedure and find the value of the maximum likelihood for the given value of n_{de} . In the end we search the grid to find the full global maximum in the 4-parameter space.

5. APPLICATION TO WMAP-DATA

Let us now discuss the results obtained with and without normalization of our signal covariance matrix (see section 4.4). We analyze the V-band (61 GHz) data map which is believed to be one of the cleanest bands in terms of foreground residuals, and recommended for cosmological analysis by the WMAP team. To this map we apply the modified WMAP KQ85 galactic skycut, removing 25% of the sky. Since we are only analyzing the largest scales no special care is taken with regards to point-source masking. We take into account the noise RMS pattern and the corresponding beam properties for the V-band. We analyze these maps out to a maximum multipole moment $\ell_{\text{max}} = 20$. The kernel matrices \mathbf{W} which emulate the effect of a skycut in harmonic space includes multipoles up to $\ell_{\text{max}} = 40$. Now that we have our data map we are ready to start the analysis.

5.1. Unnormalized covariance matrix

Performing a grid-calculation with a spectral index range of $-5 \leq n_{\text{de}} \leq 5$ with a stepsize of $\Delta n_{\text{de}} = 0.1$, where for each value of n_{de} we do a 3-dimensional search for the peak of the likelihood function using our likelihood maximization scheme described in section 4.7 we find that the likelihood for negative spectral index values are very insignificant. As we approach $n_{\text{de}} = 0$ the

and second derivatives. Due to the symmetry of the signal covariance matrix, ϖ_0 is constrained to be larger or equal to zero. A negative amplitude can always be replaced with a positive one and a shift in the angles (θ, ϕ) : $\mathbf{S}(-\varpi_0, n_{\text{de}}, \theta, \phi) = \mathbf{S}(\varpi_0, n_{\text{de}}, \pi - \theta, \pi + \phi)$. This is easily seen from the definition of the signal covariance matrix.

The gradient is computed analytically, the derivative of Eq. (41) with respect to any of the parameters in the set α is

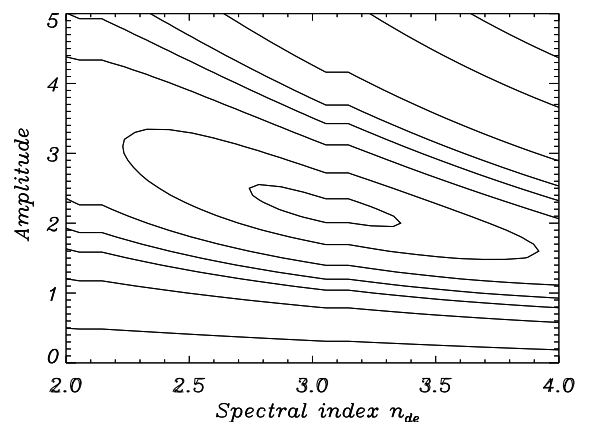


FIG. 2.— 2-dimensional plot of the raw likelihood (Posterior distribution) as a function of dark energy spectral index n_{de} and the transformed amplitude ϖ_0^a , using WMAP 7-yr data. The spherical angles have been fixed to their WMAP best-fit values at $\ell_{\text{max}} = 20$ to enable a projection. The posterior mode value is located at $n_{\text{de}} = 3.1$. The (transformed) amplitude found in this plot is higher than the value for the true anisotropic amplitude noted in table 1 due to a bias introduced by application of the mask and a linear transformation.

likelihood starts peaking slowly until we find a peak at $n_{\text{de}} = 3.1$. The best-fit direction remains practically constant as we move through the grid (the change is completely negligible compared to the uncertainty) indicating that correlation between the two sets (θ, ϕ) and $(n_{\text{de}}, \varpi_0)$ is weak.

We find Fisher matrix error bars calculating the Fisher matrix using

$$F_{\alpha\beta} = \frac{1}{2} \text{Tr} \left(\frac{d\mathbf{C}}{d\lambda_\alpha} \mathbf{C}^{-1} \frac{d\mathbf{C}}{d\lambda_\beta} \mathbf{C}^{-1} \right) \quad (43)$$

where the derivatives of the covariance matrix are found analytically for the direction and amplitude and numerically for the spectral index. Since the amplitude and spectral index are weakly correlated, the off-diagonal elements are taken into account in the matrix. The results are shown in table 1. As expected, in order for the model to be consistent with the power spectrum, we find ϖ_0 consistent with zero within the 1σ error. In figure 2 we show the likelihood surface close to the peak. Note that

² using dmng.f from www.netlib.org

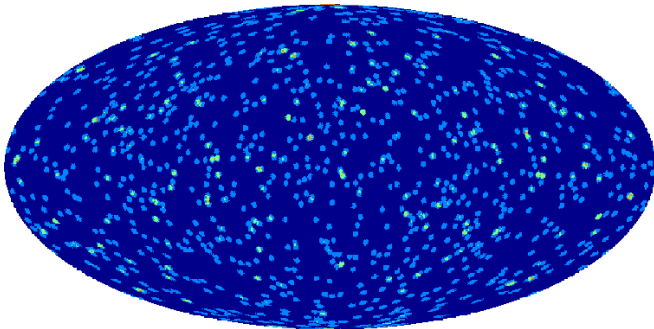


FIG. 3.— Distribution of (θ, ϕ) values on the sphere from Gaussian ($\varpi_0 = 0$ input) simulations. Note how the positions found in the simulations are randomly distributed on the sphere and not aligned along some particular axis, in clear agreement with a random Gaussian distribution.

TABLE 1
RESULTS FROM WMAP 7YR-DATA. LOWER LINE SHOWS THE RESULTS WITH NORMALIZED COVARIANCE MATRIX.

n_{de}	ϖ_0	$\hat{\mathbf{n}}(l, b)$
3.1 ± 1.5	0.51 ± 0.94	$(168^\circ, -31^\circ)$
1.2 ± 0.7	7.12 ± 3.82	$(179^\circ, -27^\circ)$

the amplitude in this plot is the transformed amplitude ϖ_0^a (see section 4.3) and that the amplitude at the maximum of the likelihood is biased with respect to the best fit amplitude. This bias results from the complicated form of the likelihood introduced by the mask. The bias is corrected for in the following manner: given the parameters found from the peak of the likelihood, we generate 100 anisotropic realisations. For each realisation we estimate the anisotropic parameters and in the end compute the average bias in ϖ_0^a . Next we subtract the bias from the input-value and repeat the procedure until our average computed amplitude matches the value found in the WMAP data. When the bias has been subtracted we are left with "the true" estimate of the transformed amplitude ϖ_0^a . The fiducial amplitude is then obtained using $\varpi_0 = \sqrt{a\varpi_0^a}$. In the unnormalized case we find a final amplitude value $\varpi_0 = 0.51$.

The best fit direction is somewhat close to the galactic center. In order to check that this is not caused by the shape of the mask, we estimated the direction on 1000 simulated isotropic maps and found that there is no bias towards the galactic center. The estimated directions are shown in figure 3.

The error in the amplitude has also been estimated using 1000 Monte Carlo simulations. We find that the error from simulations agrees well with the error found using the Fisher matrix. In figure 4 we show the best fit direction with error bars.

An isotropic universe is clearly preferred by the data using this model.

5.2. Normalized covariance matrix

The model with an unnormalized matrix (see Eq.12) giving the modified power spectrum in Eq. (35) is clearly not preferred by the WMAP 7-yr data. However, if we allow other cosmological parameters to vary we may be able to find a better fit as explained above. We have therefore repeated the procedure using the normalization in Eq. (36) which means fixing the diagonal part

wmap data map with preferred directions

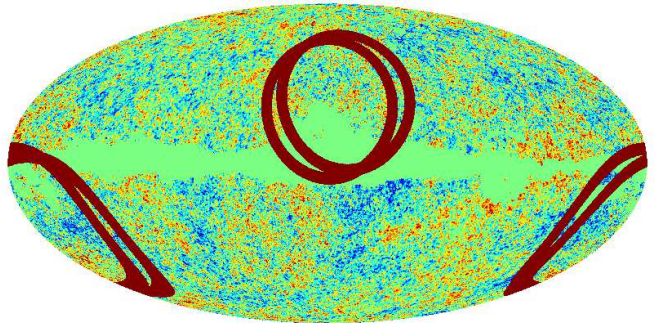


FIG. 4.— Map indicating the 1σ uncertainty in the preferred direction of the axis. The background is the V-band (61 GHz) WMAP 7-yr data map with the KQ85 mask. The two axes plotted are the directions given in table 1 for the unnormalized and the normalized cases.

of the covariance matrix to the best fit C_ℓ regardless of amplitude and spectral index.

The lower line in table 1 shows the results for the anisotropic cosmological parameters from the exploration of the likelihood space with a normalized covariance matrix. Again, a grid was set up for the spectral index in the interval $-5 \leq n_{\text{de}} \leq 5$ with the same step-size and for each value of n_{de} we estimated the best-fit values of (θ, ϕ, ϖ_0) and the corresponding value of the likelihood. The preferred amplitude in the normalized case is so large that a huge change of cosmological parameter values would be necessary to obtain the best fit WMAP spectrum. No physical solution is found in the normalized case.

6. CONCLUSIONS

In this work we tested anisotropic dark energy models with the 7-year WMAP temperature observations data. If dark energy is not a perfect fluid but for instance a vector field, the CMB sky will be distorted anisotropically on its way to us by the ISW effect. The signal covariance matrix then becomes nondiagonal for small multipoles, but at $\ell \gtrsim 20$ the anisotropy is negligible. This can be used to constrain violations of rotational invariance in the late universe, and to obtain hints on possible imperfect nature of dark energy and the large-angle anomalous features in the CMB.

To model this phenomenon, we introduced a mismatch of the two gravitational potentials in the Newtonian gauge. The mismatch, quantified by ϖ , is proportional to a gradient along the preferred axis $\hat{\mathbf{n}}$. We also allowed this effect to depend on the scale by introducing the spectral index n_{de} . Physically, such gradient could be caused by a large-scale inhomogeneity entering our horizon, spontaneous formation due to e.g. coherent magnetic fields or simply the possible imperfect nature of the dark energy field. Many possible realisations of the latter possibility were discussed in the introduction and in the section 3. The dominant effect on the CMB is then a quadrupole modulation, which has the same geometrical correlation structure but different time and scale dependence than in models considered previously. Now a dipole modulation, though subdominant, is predicted too.

We calculate the mode couplings introduced to the spherical harmonic coefficients of the CMB by the

anisotropic model and obtain the full likelihood for the lowest multipoles where the dominant contribution to the model is expected to be found. Maximizing the likelihood taking into account the instrumental parameters of the WMAP experiment, we are able to find optimal estimates of the anisotropic parameters. Analysis of the masked WMAP V-band, fixing other cosmological parameters, gave a best fit amplitude $\varpi_0 = 0.51 \pm 0.94$ and $n_{\text{de}} = 3.1$ consistent with an isotropic universe.

In comparison, test of the isotropic version of this parametrisation show that the data is then compatible with a vanishing deviation, and allows a nonzero ϖ of the order of $\mathcal{O}(0.1)$ (Daniel et al. (2010)). At the level of Solar system, no hints of deviations are observed, and the post-Newtonian correction is constrained to be at most $\mathcal{O}(10^{-5})$ (Will (2001)). However, the numbers themselves cannot be directly compared, since our best-fit model features also a strong scale-dependence of the deviation. The preferred steep blue spectral index may be due to the fact that the statistically most significant contribution must come from smaller scales, the largest scales of the CMB being severely cosmic variance limited.

Another shortcoming of our parameterization is its inability to incorporate the lack of large-angle power in the observed sky, one of the most striking anomaly present in the data. Indeed, the main lesson to be derived from our study is that cosmological constraints on realistic imperfect post-Newtonian deviations are on the order $\mathcal{O}(10^{-4})$ (reported in table 1), only an order of magnitude below those obtained from the Solar system scales. This motivates to further investigate the possible origin and constraints of imperfect source terms in cosmology. In particular, a fully consistent post-Friedmannian parametrisation along the lines of Ferreira & Skordis (2010); Baker et al. (2011), tailored to the study of directional dependence of deviations from the standard predictions of linearised cosmology, remains to be developed.

6.1. *acknowledgements*

We thank Hans Kristian Eriksen for useful discussions. The work of TK was supported by the Academy of Finland and the Yggdrasil grant from the Norwegian Research Council. DFM and FKH thank the Research Council of Norway for FRINAT grant 197251/V30 and an OYI-grant respectively. DFM is also partially supported by project PTDC/FIS/111725/2009 and CERN/FP/123618/2011. Maps and results have been derived using the Healpix³ software package developed by Gorski et al. (2005). The anisotropic transfer functions have been derived using a modified version of CAMB due to Lewis et al. (2000). We acknowledge the use of the LAMBDA archive (Legacy Archive for Microwave Background Data Analysis). Support for LAMBDA is provided by the NASA office for Space Science.

³ <http://healpix.jpl.nasa.gov>

APPENDIX

ANISOTROPIC CONTRIBUTION TO THE POWER SPECTRUM

The diagonal part of the covariance matrix is a sum of the power spectrum due to the isotropy and a term determined by the anisotropic parameters ϖ_0 , n_{de} and (θ, ϕ) :

$$S_{\ell m; \ell m} = \frac{2}{\pi} (I_\ell + \varpi_0^2 \xi_{\ell m; \ell m} I_\ell^{\text{AA}}) = C_\ell + \xi_{\ell m; \ell m} \varpi_0^2 C_\ell^{\text{AA}} \quad (\text{A1})$$

The dependence on the spectral index comes from the integral over the anisotropic transfer functions in I_ℓ^{AA} . The diagonal part of the geometric factor is (Ackerman et al. 2007)

$$\xi_{\ell m; \ell m} = -2n_+ n_- \frac{-1 + \ell(\ell+1) + m^2}{(2\ell-1)(2\ell+3)} + n_0^2 \frac{2\ell(\ell+1) - 2m^2 - 1}{(2\ell-1)(2\ell+3)} \quad (\text{A2})$$

where the spherical components n_+ , n_- , n_0 containing the angular dependence have been defined in Equation (10). Using the well-known result

$$\sum_{m=-\ell}^{\ell} m^2 = \frac{\ell(\ell+1)(2\ell+1)}{6} \quad (\text{A3})$$

we find that the average of the geometric factor is free from angular dependence and simplifies nicely to

$$\sum_{m=-\ell}^{\ell} \xi_{\ell m; \ell m} = \frac{2\ell+1}{3} \quad (\text{A4})$$

With this result one finds that the theoretical prediction for the modified power spectrum due to the anisotropic component becomes

$$C_\ell^{\text{mod}} = \frac{1}{2\ell+1} \sum_m \langle a_{\ell m} a_{\ell m}^* \rangle = C_\ell + \frac{\varpi_0^2}{3} C_\ell^{\text{AA}} \quad (\text{A5})$$

which is the modified power spectrum C_ℓ^{mod} quoted in Eq. (35).

REFERENCES

- Abramo, L. R., & Pereira, T. S. 2010, arXiv: 1002.3173 [astro-ph.CO]
Ackerman, L., Carroll, S. M., & Wise, M. B. 2007, Phys. Rev., D75, 083502
Adamek, J., Campo, D., & Niemeyer, J. C. 2010, arXiv: 1003.3204 [hep-th]
Afshordi, N., Geshnizjani, G., & Khoury, J. 2009, JCAP, 0908, 030
Akarsu, O., & Kilinc, C. B. 2010, Gen. Rel. Grav., 42, 763
Aluri, P. K., & Jain, P. 2011, arXiv: 1108.5894 [astro-ph.CO]
Appleby, S., Battye, R., & Moss, A. 2010, Phys. Rev., D81, 081301
Armendariz-Picon, C. 2004, JCAP, 0407, 007
Armendariz-Picon, C., & Pekowsky, L. 2008, 0807.2687
Baker, T., Ferreira, P. G., Skordis, C., & Zuntz, J. 2011, arXiv: 1107.0491 [astro-ph.CO]
Battye, R., & Moss, A. 2009, Phys. Rev., D80, 023531
Bennett, C. L., et al. 2003, Astrophys. J. Suppl., 148, 1
Boehmer, C. G., & Mota, D. F. 2008, Phys. Lett., B663, 168
Caldwell, R., Cooray, A., & Melchiorri, A. 2007, astro-ph/0703375
Campanelli, L. 2009, Phys. Rev., D80, 063006
Cooke, R., & Lynden-Bell, D. 2009, arXiv: 0909.3861 [astro-ph.CO]
Cooray, A. R., Holz, D. E., & Caldwell, R. 2008, astro-ph/0812.0376
Copi, C. J., Huterer, D., Schwarz, D. J., & Starkman, G. D. 2010, arXiv: 1004.5602 [astro-ph.CO]
Daniel, S. F., Caldwell, R. R., Cooray, A., & Melchiorri, A. 2008, Phys. Rev., D77, 103513
Daniel, S. F., Caldwell, R. R., Cooray, A., Serra, P., & Melchiorri, A. 2009, 0901.0919
Daniel, S. F., et al. 2010, arXiv: 1002.1962 [astro-ph.CO]
Dimastrogiovanni, E., Fischler, W., & Paban, S. 2008, JHEP, 07, 045
Dimopoulos, K., Karcauskas, M., & Wagstaff, J. M. 2010, Phys. Rev., D81, 023522
Dimopoulos, K., Wills, D., & Zavala, I. 2011, arXiv: 1108.4424 [hep-th]
Dvali, G. R., Gabadadze, G., & Porrati, M. 2000, Phys. Lett., B485, 208
Erickcek, A. L., Kamionkowski, M., & Carroll, S. M. 2008, Phys. Rev., D78, 123520
Eriksen, H. K., Hansen, F. K., Banday, A. J., Gorski, K. M., & Lilje, P. B. 2004, Astrophys. J., 605, 14
Ferreira, P. G., & Skordis, C. 2010, arXiv: 1003.4231 [astro-ph.CO]
Germani, C., & Kehagias, A. 2009, JCAP, 0903, 028
Golovnev, A., Mukhanov, V., & Vanchurin, V. 2008, JCAP, 0806, 009
Gordon, C., Hu, W., Huterer, D., & Crawford, T. M. 2005, Phys. Rev., D72, 103002
Gorski, K. M., et al. 2005, Astrophys. J., 622, 759
Graham, P. W., Harnik, R., & Rajendran, S. 2010, arXiv: 1003.0236 [hep-th]
Groeneboom, N., Axelsson, M., Mota, D., & Koivisto, T. 2010, arXiv: 1011.5353 [astro-ph.CO]
Groeneboom, N. E., Axelsson, M., Mota, D. F., & Koivisto, T. 2010, ArXiv e-prints
Groeneboom, N. E., & Eriksen, H. K. 2008, 0807.2242
Gumrukcuoglu, A. E., Contaldi, C. R., & Peloso, M. 2006, astro-ph/0608405
—. 2007, JCAP, 0711, 005
Hansen, F. K., Banday, A. J., Gorski, K. M., Eriksen, H. K., & Lilje, P. B. 2008, 0812.3795
Hinshaw, G., et al. 2007, Astrophys. J. Suppl., 170, 288
Hoftuft, J., et al. 2009, 0903.1229
Hu, W., & Sawicki, I. 2007, Phys. Rev., D76, 104043
Jimenez, J. B., Koivisto, T. S., Maroto, A. L., & Mota, D. F. 2009, JCAP, 0910, 029
Jimenez, J. B., & Maroto, A. L. 2008, Phys. Rev., D78, 063005
—. 2009a, JCAP, 0903, 016
—. 2009b, 0903.4672
Kiselev, V. V. 2004, Class. Quant. Grav., 21, 3323
Koivisto, T., & Mota, D. F. 2006, Phys. Rev., D73, 083502
—. 2008a, JCAP, 0806, 018
Koivisto, T. S., & Mota, D. F. 2008b, JCAP, 0808, 021
—. 2011, JHEP, 1102, 061
Koivisto, T. S., Mota, D. F., & Pitrou, C. 2009, 0903.4158
Koivisto, T. S., Mota, D. F., Quartin, M., & Zlosnik, T. G. 2011, Phys. Rev., D83, 023509
Koivisto, T. S., & Nunes, N. J. 2009, Phys. Rev., D80, 103509
Land, K., & Magueijo, J. 2005, Phys. Rev. Lett., 95, 071301

- Lewis, A., Challinor, A., & Lasenby, A. 2000, *Astrophys. J.*, 538, 473
- Li, B., Fonseca Mota, D., & Barrow, J. D. 2008, *Phys. Rev.*, D77, 024032
- Libanov, M., Rubakov, V., Papantonopoulos, E., Sami, M., & Tsujikawa, S. 2007, *JCAP*, 0708, 010
- Manera, M., & Mota, D. 2006, *Mon.Not.Roy.Astron.Soc.*, 371, 1373
- Mota, D. F., Kristiansen, J. R., Koivisto, T., & Groeneboom, N. E. 2007, *Mon. Not. Roy. Astron. Soc.*, 382, 793
- Pereira, T. S., Pitrou, C., & Uzan, J.-P. 2007, *JCAP*, 0709, 006
- Prunet, S., Uzan, J.-P., Bernardeau, F., & Brunier, T. 2005, *Phys. Rev.*, D71, 083508
- Rakic, A., & Schwarz, D. J. 2007, *Phys. Rev.*, D75, 103002
- Rodrigues, D. C. 2008, *Phys. Rev.*, D77, 023534
- Rubakov, V. A. 2006, *Theor. Math. Phys.*, 149, 1651
- Skordis, C. 2009, *Phys. Rev.*, D79, 123527
- Tangen, K. 2009, arxiv: 0910.4164 [astro-ph.CO]
- Will, C. M. 2001, *Living Rev. Rel.*, 4, 4
- Zlosnik, T. 2011, arXiv: 1107.0389 [gr-qc]
- Zuntz, J., Zlosnik, T. G., Bourliot, F., Ferreira, P. G., & Starkman, G. D. 2010, arxiv: 1002.0849 [astro-ph.CO]